Available online at www.sciencedirect.com
ScienceDirect
Journal of Sound and Vibration 318 (2008) 461–487
JOURNAL OF SOUND AND VIBRATION
www.elsevier.com/locate/jsvi

On the correct representation of bending and axial deformation in the absolute nodal coordinate formulation with an elastic line approach

Johannes Gerstmayr[a,*], Hans Irschik[b,1]

[a]*Linz Center of Mechatronics, Altenbergerstr. 69, 4040 Linz, Austria*
[b]*Institute of Technical Mechanics, University of Linz, Altenbergerstr. 69, 4040 Linz, Austria*

Received 11 January 2008; received in revised form 21 March 2008; accepted 15 April 2008
Handling Editor: A.V. Metrikine
Available online 12 June 2008

Abstract

In finite element methods that are based on position and slope coordinates, a representation of axial and bending deformation by means of an elastic line approach has become popular. Such beam and plate formulations based on the so-called absolute nodal coordinate formulation have not yet been verified sufficiently enough with respect to analytical results or classical nonlinear rod theories. Examining the existing planar absolute nodal coordinate element, which uses a curvature proportional bending strain expression, it turns out that the deformation does not fully agree with the solution of the geometrically exact theory and, even more serious, the normal force is incorrect. A correction based on the classical ideas of the extensible elastica and geometrically exact theories is applied and a consistent strain energy and bending moment relations are derived. The strain energy of the solid finite element formulation of the absolute nodal coordinate beam is based on the St. Venant–Kirchhoff material: therefore, the strain energy is derived for the latter case and compared to classical nonlinear rod theories. The error in the original absolute nodal coordinate formulation is documented by numerical examples. The numerical example of a large deformation cantilever beam shows that the normal force is incorrect when using the previous approach, while a perfect agreement between the absolute nodal coordinate formulation and the extensible elastica can be gained when applying the proposed modifications. The numerical examples show a very good agreement of reference analytical and numerical solutions with the solutions of the proposed beam formulation for the case of large deformation pre-curved static and dynamic problems, including buckling and eigenvalue analysis. The resulting beam formulation does not employ rotational degrees of freedom and therefore has advantages compared to classical beam elements regarding energy-momentum conservation.

1. Introduction

The pioneering paper of Simo and Vu-Quoc [1] showed that the simulation of large deformation beam problems for multibody system dynamics is feasible. The so-called geometrically exact beam formulation of

*Corresponding author. Tel.: +43 732 2468 9762; fax: +43 732 2468 9763.
E-mail addresses: johannes.gerstmayr@jku.at (J. Gerstmayr), hans.irschik@jku.at (H. Irschik).
[1]Tel.: +43 732 2468 9761; fax: +43 732 2468 9763.

0022-460X/$ - see front matter © 2008 Elsevier Ltd. All rights reserved.
doi:10.1016/j.jsv.2008.04.019

the strain energy of Simo and Vu-Quoc's beam elements is based on classical nonlinear rod theories of Reissner [2] and Antman [3]. It coincides with the strain definitions in the Euler elastica [4], if shear deformation is neglected. The numerical treatment of geometrically exact beam elements is based on discretization of the position of the beam centerline and rotation of the cross section. The strain energy can be interpreted with the help of a corotational formulation of the strain: see Géradin and Cardona [5].

Alternatively, the absolute nodal coordinate formulation (ANCF) is a large deformation finite element formulation which utilizes nodal displacement and slope degrees of freedom for the interpolation of the displacement field of beam elements: see Shabana [6]. A substantial number of publications, numerical simulations and verification of physical experiments show advantages of the absolute nodal coordinate formulation and the ability to solve large deformation problems, e.g. in the field of multibody system dynamics, with correct rigid body inertia terms [7]. The ANCF finite elements with a high order of interpolation in the axial direction are similar to solid finite elements, but are utilized as beam or plate elements and therefore some of the ANCF elements suffer from locking. As one of the main advantages, the ANCF leads to a constant mass matrix, which is different from the spatial case of the geometrically exact beam formulation of Simo and Vu-Quoc [8]. As a second advantage, the local differential equilibrium follows immediately from equations of the three-dimensional continuum, simply equilibrating inertia forces with the divergence of the first Piola Kirchhoff stress and external forces. The work of elastic forces can be directly derived from any linear or nonlinear material law known from continuum mechanics: see e.g. Ref. [9]. Frequently, the linear elastic, St. Venant–Kirchhoff material based on the Green Lagrange strain and the second Piola Kirchhoff stress is utilized. The latter material definition is usually applied in fully three-dimensional solid finite elements, but it is different from the material law incorporated into the classical elastica or Reissner's beam theory. For this reason, the axial and bending strain of a beam theory based on the St. Venant–Kirchhoff material is outlined in Appendix A, which shows the differences from the classical elastica theory. As a third advantage, ANCF elements immediately employ continuity of gradients along and between adjacent elements, which is e.g. of great advantage in fluid–structure interaction [10] or sliding joint applications.

Fully parameterized finite elements based on the ANCF show various types of locking, such as Poisson locking, see Sopanen and Mikkola [11], as well as combined shear and thickness locking: see Gerstmayr and Shabana [12]. The numerous types of locking can be resolved and, afterwards, lead to good agreement with the solution of fully three-dimensional computations with solid finite elements: see Ref. [13]. Original ANCF finite elements [7] relax the kinematic constraints of the Timoshenko beam theory, by including cross-section deformation. While this extended beam theory is interesting for large deformation of rubber-like structures or large strain elasto-plasticity in rolling problems, the cross-section deformation requires additional degrees of freedom as compared to geometrically exact approaches and leads to a larger number of computations in the elastic forces. An efficient numerical scheme to solve dynamic problems based on absolute nodal coordinates with small deformation but large overall motion has been proposed by Gerstmayr and Schöberl [14] and extended to modal reduction methods by Gerstmayr and Ambrósio [15].

As an alternative to fully parameterized ANCF elements, there are simplified ANCF elements which only take into account the deformation of the elastic line of the beam element [16,12,17]. The latter so-called elastic line formulation is computationally more efficient, but less general. In the Bernoulli–Euler ANCF beam or cable elements of Berzeri and Shabana [16] and Gerstmayr and Shabana [12], only nodal positions and axial slopes are utilized to discretize displacements. In the extended formulation of Schwab and Meijaard [17], the three-dimensional case is studied including shear deformation. In a recent investigation regarding the verification of ANCF finite elements by comparison to analytical solution and classical corotational approaches, see Dibold et al. [18], it turned out that the elastic line elements were inappropriately formulated. The results did not coincide fully with analytical results and, as is demonstrated subsequently, the normal forces are erroneous.

The present paper focuses on the consistent treatment of the virtual work of elastic forces in the ANCF with an elastic line approach. Two approaches are examined. The first, and proposed approach is based on the classical extensible elastica [4], which is identical to Reissner's formulation [2], if shear deformation is disregarded. We derive the virtual work of elastic forces of the three-dimensional continuum with an elastic material law which is linear in Biot's strain. This leads to classical decoupled axial and bending strain terms in

the strain energy. It is shown that the proposed consistent strain terms are different from the formulation of Berzeri and Shabana [16], which leads to wrong stress resultants and buckling loads and requires more nonlinear iterations. In the second approach, a St. Venant–Kirchhoff elastic material is used to derive the virtual work of a large deformation beam element. This approach is fundamentally different from the elastica or Reissner's approach and can be derived from the three-dimensional continuum without any geometrical approximations other than the Bernoulli–Euler constraints. Thus, the second approach is understood to be geometrically exact as well. The St. Venant–Kirchhoff approach clarifies the kinematic relations which are embedded in the original fully parameterized ANCF elements, compare with Yakoub and Shabana [7], and incorporates a quadratic distribution of strain along the cross section of the beam. The St. Venant–Kirchhoff approach leads to highly coupled strain energy regarding the strain of the beam centerline and the curvature of the beam axis. This approach includes an additional fourth moment of area in the bending strain energy and it is therefore understood as an approach that is inconvenient for engineering applications, because it includes many nonlinear terms and it requires specific boundary conditions. The difference of the St. Venant–Kirchhoff approach as compared to the elastica is very small, even in large deformation applications and depends on the height and curvature of the beam. Details of this approach are included in the appendix of the present paper, because they can help to understand the fully parameterized ANCF elements. A recent discussion of Reissner's nonlinear rod theory and the relation to the three-dimensional continuum is given by Gerstmayr and Irschik [19].

The proposed finite elements, which are based on the classical nonlinear rod theory, are verified by means of detailed numerical examples and comparison to analytical results of a large deformation cantilever, which could be retrieved in the symbolic computation package MAPLE [20]. Classical examples, such as the post-buckling behavior of a 215° arch, the large deformation bending of a half-circle beam and the eigenvalues of a ring, show that the proposed formulation is appropriate to exactly reproduce classical results. Last but not least, a highly dynamic, large deformation example is utilized to show the advantages in dynamic applications.

2. Original planar ANCF element

In the following, we consider the planar ANCF element proposed by Berzeri and Shabana [16]. Well in line with the Bernoulli–Euler beam theory, the ANCF finite element considers only axial and bending, but no shear deformation. Large deformations and large rotations are considered in the formulation of the equations of motion for the element. There are several ways to describe the undeformed and deformed configuration of the beam. The conventional way to model the beam axis of a classical elastica or a slender rod would use the angle θ to describe the rotation of the cross section of the deformed beam, see e.g. Love [4], and for the extension to shear deformable beams; see Antman [3] and Reissner [2]. The alternative way to model the deformation of the beam axis here is to use a polynomial interpolation of the beam axis, such as in the ANCF. The advantage of such a formulation is a simple expression for the inertia terms, which leads to a constant mass matrix and avoids nonlinear coupling in the inertia terms even in the case of three-dimensional motion and deformation. Furthermore, the elastic forces have a standard form like in iso-parametric solid finite elements which allows the application of numerical methods and material laws which are widely known. The ANCF elements are especially designed for multibody dynamic system simulation and offer therefore an easy formulation of constraints at nodal points. An extension to fluid–structure interaction [10] or multiphysics problems is straightforward, because the position of a point at the deformed beam axis is given by a simple polynomial expression.

The position vector $\mathbf{r}$ describing the position in the deformed configuration, originally placed at x of the undeformed beam axis, see Fig. 1, is interpolated by shape functions $\mathbf{S}$ and element coordinates $\mathbf{q}$

$$\mathbf{r} = \mathbf{S}\mathbf{q} \tag{1}$$

In order to connect such beam elements rigidly and in order to apply constraints, it is advantageous to use nodal position and slopes as the nodal coordinates. The coordinates of node j are denoted as

$$\mathbf{q}^{(j)} = [\mathbf{r}^{\mathrm{T}}|_j \;\; \mathbf{r}'^{\mathrm{T}}|_j]^{\mathrm{T}} \tag{2}$$

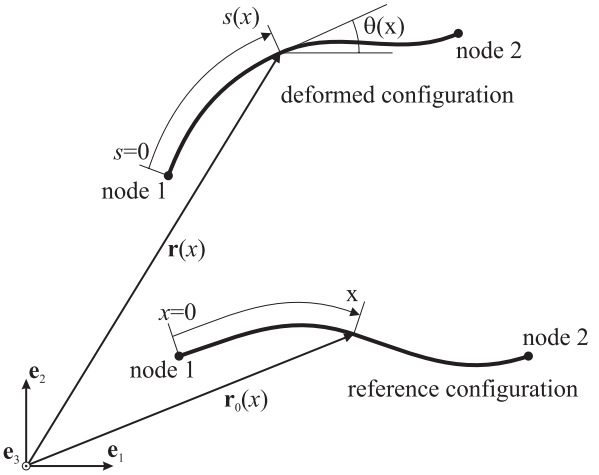

Fig. 1. Reference and deformed configuration of the planar ANCF element.

The abbreviation for the spatial derivative of $\mathbf{r}$ is given by

$$\mathbf{r}' = \frac{\partial \mathbf{r}}{\partial x} \tag{3}$$

The element coordinates are denoted as

$$\mathbf{q} = [\mathbf{q}^{(1)^{\mathrm{T}}} \ \mathbf{q}^{(2)^{\mathrm{T}}}]^{\mathrm{T}} \tag{4}$$

Thus, a two-noded planar element has eight degrees of freedom. For the two-noded element, the interpolation space of the beam axis is defined by two third-order polynomials in x,

$$\mathbf{r} = \begin{bmatrix} r_x \\ r_y \end{bmatrix} = \begin{bmatrix} a_0 + a_1 x + a_2 x^2 + a_3 x^3 \\ b_0 + b_1 x + b_2 x^2 + b_3 x^3 \end{bmatrix} \tag{5}$$

This interpolation allows coupled bending and stretch of the beam axis, while shear is not included. The unknown coefficients a_i and b_i are substituted by the nodal coordinates in the following. An extension of ANCF elements to shear deformation together with an interpolation of the cross section can be found in the literature [21].

Inserting Eqs. (2) and (5) into Eq. (1), the shape function matrix $\mathbf{S}_m$ can be determined

$$\mathbf{r} = [S_1\mathbf{I} \ S_2\mathbf{I} \ S_3\mathbf{I} \ S_4\mathbf{I}]\mathbf{q} = \mathbf{S}_m\mathbf{q} \tag{6}$$

where $\mathbf{I}$ is the 2×2 unit matrix. The single shape functions S_i are given by

$$\begin{aligned} S_1 &= 1 - 3\frac{x^2}{L^2} + 2\frac{x^3}{L^3}, \quad S_2 = x - 2\frac{x^2}{L} + \frac{x^3}{L^2} \\ S_3 &= 3\frac{x^2}{L^2} - 2\frac{x^3}{L^3}, \quad S_4 = -\frac{x^2}{L} + \frac{x^3}{L^2} \end{aligned} \tag{7}$$

where the beam coordinate $x \in [0, L]$ can be transformed into a normalized coordinate $\xi = 2x/L - 1$ with $\xi \in [-1, +1]$. This allows a conventional numerical integration for the normalized element coordinate ξ. The position vector of a point at a distance $y \in [-H/2, H/2]$ from the beam axis in the deformed configuration reads according to the Bernoulli–Euler theory,

$$\mathbf{p}(x) = \mathbf{r}(x) + y\mathbf{n}(x) \tag{8}$$

where $\mathbf{n}$ denotes the normal vector to the beam axis at x, given by

$$\mathbf{n} = \frac{1}{|\mathbf{r}'|}\begin{bmatrix} -r'_y \\ r'_x \end{bmatrix} \tag{9}$$

2.1. Equations of motion

The weak forms of the equations of motion are derived from the Lagrange–D'Alembert equation,

$$\delta W_I + \delta W_S - \delta W_E = 0 \tag{10}$$

where δW_I denotes the virtual work of inertia forces, δW_S is the virtual work of internal (elastic) forces and δW_E is the virtual work of external forces.

The mass matrix is determined from the kinetic energy

$$\begin{aligned} T &= \frac{1}{2}\int_V \rho \dot{\mathbf{r}}^{\mathrm{T}}\dot{\mathbf{r}}\,\mathrm{d}V = \frac{1}{2}\int_L \rho A \dot{\mathbf{r}}^{\mathrm{T}}\dot{\mathbf{r}}\,\mathrm{d}x \\ &= \dot{\mathbf{q}}^{\mathrm{T}}\int_0^L \rho A\left(\frac{\partial \mathbf{r}}{\partial \mathbf{q}}\right)^{\mathrm{T}}\frac{\partial \mathbf{r}}{\partial \mathbf{q}}\,\mathrm{d}x\dot{\mathbf{q}} = \dot{\mathbf{q}}^{\mathrm{T}}\int_0^L \rho A \mathbf{S}_m^{\mathrm{T}}\mathbf{S}_m\,\mathrm{d}x\dot{\mathbf{q}} = \dot{\mathbf{q}}^{\mathrm{T}}\mathbf{M}\dot{\mathbf{q}} \end{aligned} \tag{11}$$

and leads to

$$\mathbf{M} = \int_0^L \rho A \mathbf{S}_m^{\mathrm{T}}\mathbf{S}_m\,\mathrm{d}x \tag{12}$$

where $\mathbf{S}_m$ is according to the shape matrix defined in Eq. (6), A denotes the cross-sectional area of the beam element and ρ is the density. The mass matrix is constant and can be stored in sparse form. The kinetic energy of Eq. (11) coincides with the form provided by Simo and Vu-Quoc [1], except for the rotation of the cross section which can be neglected in the present Bernoulli–Euler theory.

The virtual work of inertia forces is finally given by

$$\delta W_I = \ddot{\mathbf{q}}^{\mathrm{T}}\mathbf{M}\delta\mathbf{q} \tag{13}$$

The virtual work of external forces for a space-wise constant body force $\mathbf{b}$ is given by

$$\delta W_E^b = \int_L A\mathbf{b}^{\mathrm{T}}\delta\mathbf{r}(x)\,\mathrm{d}x \tag{14}$$

and the work of a torque M at a point x is

$$\delta W_E^M = M\delta\theta(x) \tag{15}$$

where $\theta(x)$ denotes the rotation of the deformed beam axis of a point P, originally located at x in the undeformed configuration; see Fig. 1.

3. Virtual work of elastic forces

The main contribution of the present paper concerns the detailed discussion of the work of elastic forces. We first present the original formulation of Berzeri and Shabana [16], perform a term-wise comparison with classical nonlinear rod theories and derive the correct curvature relations with the help of the Biot strain tensor.

3.1. Strain energy and elastic forces as proposed by Berzeri and Shabana [16]

The original expression for the strain energy (work of elastic forces) as provided by Berzeri and Shabana reads

$$W_S^B = \frac{1}{2}\int_0^L (EA(\varepsilon_{11}^0)^2 + EI\kappa^2)\,\mathrm{d}x \tag{16}$$

The axial stiffness is represented by $EA = \int_{-H/2}^{H/2} WE \, \mathrm{d}y$ and the bending stiffness is $EI = \int_{-H/2}^{H/2} WEy^2 \, \mathrm{d}y$. The authors of Ref. [16] presented several approximations of the axial strain at the beam axis ε_{11}^0 and the curvature κ. The most general expressions provided by Berzeri and Shabana are

$$\varepsilon_{11}^0 = \tfrac{1}{2}(\mathbf{r}'^{\mathrm{T}}\mathbf{r}' - 1) \tag{17}$$

and

$$\kappa = \frac{|\mathbf{r}' \times \mathbf{r}''|}{|\mathbf{r}'|^3} \tag{18}$$

where ε_{11}^0 denotes the axial (xx) component of the Green strain tensor and κ denotes the actual curvature of the space curve described by $\mathbf{r}$. As can be seen in Appendix A, a derivation of the beam kinematics from the Green strain requires a more complicated expression for the strain energy due to axial deformation as compared to Eq. (17), see Eq. (83), and the bending deformation is approximately proportional to $|\mathbf{r}'|^2\kappa$ rather than κ. A pure formulation based on the Green strain is cumbersome and the bending strain is completely different from Eq. (16); cf. Eq. (83). This is the reason why the strain energy is derived in an alternative way, see Section 3.3.1, subsequently.

Berzeri and Shabana provide a relation of the resultant couple M and the curvature by means of

$$M = EI\kappa \tag{19}$$

and a resultant force could be defined as

$$F = EA\varepsilon_{11}^0 \tag{20}$$

The latter equation is not derived from the integration over the cross section, because in this theory, no information is given about the local stress–strain behavior within the cross section. Needless to say, it makes no sense to combine a strain at the cross section derived from Eq. (8) with the bending moment of Eq. (19), because the result contradicts with Eq. (81) given in the Appendix.

It should be mentioned that Berzeri and Shabana [16] provided simplifications of Eqs. (17) and (18), such as approximating the curvature for the case of small axial deformation,

$$\kappa \approx |\mathbf{r}''| \tag{21}$$

Similar assumptions can already be found in the classical work of Love [4, p. 384], where the approximation $|\mathbf{r}'| \approx 1$ is used. Unfortunately, Eq. (21) does not lead to correct results, when taking into account axial deformation. There have been even more rough approximations of the axial strain [22], such as using the distance of the nodes of a finite element,

$$\varepsilon_{11}^0 \approx \frac{d-l}{l} \quad \text{with } d = |\mathbf{r}_2 - \mathbf{r}_1| \tag{22}$$

where $\mathbf{r}_j$ denotes the nodal position of node j.

In the following we focus on the more general formulation for axial and bending deformation, as given by Eqs. (17) and (18), while it has been numerically tested that the simplified expressions, for example the simplified curvature of Eq. (21), do not resolve the discussed problems.

3.2. Critical discussion of the strain energy for coupled bending and axial deformation

There is a large history of formulations to describe large deformation beam elements. Unfortunately, many works either consider the inextensible axis, as in the inextensible elastica, see Chapter 19 of [4], or an extensible axis together with shear deformation [2], which practically involves the case of the extensible elastica. In the present section, the formulation is consistent with the theory on the shear deformable beam formulation of Reissner [2]; however, we assume the shear deformation to be identically zero. Concerning the classical elastica, which does not take into account axial deformation, already Bernoulli and Euler [4] stated that the bending moment is proportional to the curvature of the deformed beam axis and that the work done in

bending a rod is proportional to the square of the curvature. However, this result is only valid for the case of the inextensible axis.

The fact that the (geometrical) curvature depends on the change in stretch leads to erroneous results if the bending strain energy is quadratic in the curvature of the deformed beam. This fact is well known from the literature, see e.g. the discussion of Antman [23, p. 88]. The correct term to describe bending independently of axial stretch is usually derived from the local equilibrium equation for an initial beam segment $\mathrm{d}x$ that is stretched to $\mathrm{d}s = \lambda\,\mathrm{d}x$.

3.2.1. Example of a cantilever beam with end moment

A simple example of a cantilever beam with a bending moment M_L applied at the free end is used in order to demonstrate the problem of Eq. (16). The work of external forces for a tip bending moment reads

$$\delta W_E = M_L \delta\theta_L \tag{23}$$

where θ_L denotes the angle of rotation of the free end of the cantilever with respect to the reference configuration. The local curvature of the beam can be either written with respect to the (deformed) arc length parameter s or with respect to the beam reference coordinate x: for a derivation see e.g. Gerstmayr and Shabana [12],

$$\kappa = \frac{\partial\theta}{\partial s} = \frac{\partial\theta}{\partial x}\left(\frac{\partial s}{\partial x}\right)^{(-1)} =: \frac{K}{\lambda} \tag{24}$$

Here, λ denotes the stretch of the beam axis

$$\lambda = \frac{\partial s}{\partial x} = \sqrt{\mathbf{r}'^{\mathrm{T}}\mathbf{r}'} = |\mathbf{r}'| \tag{25}$$

In the following, we show that the choice of a bending strain is sensitive to small approximations regarding the axial strain. The quantity K is often described in the literature with the Greek symbol κ, although it is not the curvature. Some people try to avoid a name for K, while Reissner [2] denotes K as a bending strain, Simo and Vu-Quoc [1] describe K as 'rate of rotation of the cross section along the undeformed length of the beam' and Géradin and Cardona [5] interpret K as the *material measure of curvature*. In accordance to the latter definition, it might be advantageous to distinguish κ by denoting it as the *spatial measure of* curvature or the *geometrical* curvature.

The angle of rotation of the beam tip can be rewritten in terms of K,

$$\theta_L = \int_0^L \frac{\partial\theta}{\partial x}\,\mathrm{d}x = \int_0^L K\,\mathrm{d}x \tag{26}$$

According to the classical beam theory, we assume that the stretch and the change of rotation is constant along the beam axis. The angle thus follows the simple relation:

$$\theta_L = LK = \kappa\lambda L \tag{27}$$

The virtual work of internal and external forces according to Eq. (16) is

$$\delta W_S - \delta W_E = \int_0^L (EA(\lambda-1)\delta\lambda + EI(\kappa-\kappa_0)\delta\kappa)\,\mathrm{d}x - M_L\delta\theta_L = 0 \tag{28}$$

where the axial strain has been replaced by $\varepsilon_{11}^0 = \lambda - 1$, which is a good approximation of the Green strain of the original formulation of Berzeri and Shabana [16], for the error analysis in the case of small strains. The initial curvature κ_0 is considered in Eq. (28) in order to derive the more general case of pre-deformed beams. Assuming λ and κ in Eq. (28) to be constant along the beam length, the relations follow for the Berzeri–Shabana formulation as

$$(EA\lambda - M_L\kappa)\delta\lambda = 0,$$

$$(EI(\kappa-\kappa_0) - M_L(1+\lambda))\delta\kappa = 0 \tag{29}$$

with the solution

$$\lambda = \frac{M_L(EI\kappa_0 + M_L)}{EAEI - M_L^2} \approx \frac{M_L(EI\kappa_0 + M_L)}{EAEI} = \kappa_{ex}(\kappa_{ex} - \kappa_0)\frac{EI}{EA},$$

$$\kappa = \frac{EA(EI\kappa_0 + M_L)}{EAEI - M_L^2} \tag{30}$$

The geometrically correct values should be $\lambda_{ex} = 0$ and $\kappa_{ex} = M_L/EI$, which follow, if we use K instead of κ in Eq. (28). The approximation of λ in Eq. (30) holds for large axial stiffness. On the other hand, the erroneous stretch becomes larger if the axial stiffness approaches the bending stiffness. Even if this derivation assumes only constant strain and curvature along the beam axis, the results agree very well with the numerical results of Section 4.3. The results of Eq. (30) can be used to estimate the error in infinitesimally short beam segments as well.

3.3. Derivation of the virtual work of elastic forces in a beam element

The derivation of Reissner's shear deformable beam formulation is based on the virtual work and the differential equilibrium equations at the level of beam formulations, i.e. no strain or stress tensors are addressed in Ref. [2]. In contrast, we are able to utilize a more convenient approach based on the three-dimensional Biot strain in the case of the Bernoulli–Euler beam theory. This formulation is in line with the description of Reissner's beam formulation given in the monograph of Géradin and Cardona [5, p. 110], which is based on a pseudo-polar decomposition for the deformation gradient. Alternatively, a beam formulation based on a linear stress–strain relation in the Green strain and the second Piola Kirchhoff stress leads to a nonlinear distribution of strain with respect to the height of the beam: see Fig. 2 and Appendix A for more detailed expressions.

We start with the kinematic relations of a Euler–Bernoulli beam. An undeformed position of a point P in reference configuration is defined by the axial coordinate $x \in [0, L]$ and the normal distance $y \in [-H/2, H/2]$ from the beam centerline: see Fig. 3. The deformed position of point P is described by

$$\mathbf{p}(x) = \mathbf{r}(x) + y\mathbf{t}_2(x) \tag{31}$$

Here, $\mathbf{r}$ denotes the position of the beam axis and $\mathbf{t}_2$ is the unit normal vector which represents the cross section and which is perpendicular to the beam axis: see Fig. 3. A so-called moving basis, given by the vectors $\mathbf{t}_i$, is attached to the beam cross section. The vector $\mathbf{t}_3$ is perpendicular to the plane of deformation and the following relations hold:

$$\mathbf{t}_1 = \frac{1}{|\mathbf{r}'|}\frac{\partial \mathbf{r}}{\partial x}, \quad \mathbf{t}_1^{\mathrm{T}}\mathbf{t}_2 = 0, \quad \mathbf{t}_1^{\mathrm{T}}\mathbf{t}_3 = 0 \quad \text{and} \quad \mathbf{t}_2^{\mathrm{T}}\mathbf{t}_3 = 0 \tag{32}$$

For later use, we define the rotation matrix

$$\mathbf{A} = \mathbf{t}_1 \otimes \mathbf{e}_1 + \mathbf{t}_2 \otimes \mathbf{e}_2 + \mathbf{t}_3 \otimes \mathbf{e}_3 \tag{33}$$

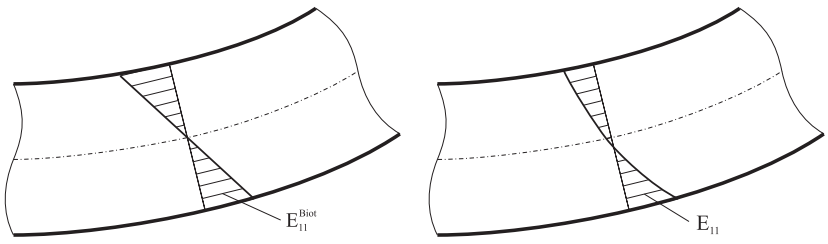

Fig. 2. Sketch of the distribution of axial strain versus beam height in pure bending for the case of Biot and Green strain.

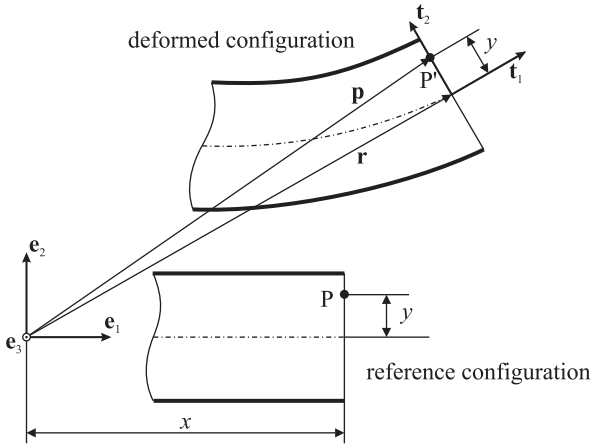

Fig. 3. Definition of the deformed Bernoulli–Euler beam and the moving vectors $\{\mathbf{t}_1, \mathbf{t}_2\}$.

The derivative of the position vector $\mathbf{p}$ with respect to x is given by

$$\mathbf{p}' = \frac{\partial \mathbf{p}}{\partial x} = \mathbf{r}' + y\mathbf{t}_2' \tag{34}$$

and the derivative of the normal vector $\mathbf{t}_2$ is computed from the well-known differential geometric relation

$$\mathbf{t}_2' = -\theta' \mathbf{t}_1 \tag{35}$$

where the rate of change of rotation with respect to the undeformed beam axis is defined as, see also Eq. (24),

$$\theta' = \frac{\partial \theta}{\partial s}\frac{\partial s}{\partial x} = \kappa \frac{\partial s}{\partial x} = K = \left(\frac{\mathbf{r}' \times \mathbf{r}''}{|\mathbf{r}'|^2}\right)^{\mathrm{T}} \mathbf{e}_3 \tag{36}$$

Note that κ does not represent the classical curvature, because it can also take on negative values. However, for the planar case, it is convenient to use this formula. Direct calculation of $\mathbf{t}_2'$ takes a cumbersome form, but can be utilized to verify the derivation of the strain energy,

$$\mathbf{t}_2' = \frac{1}{|\mathbf{r}'|}\begin{bmatrix} -\mathbf{r}''^{\mathrm{T}}\mathbf{e}_2 \\ \mathbf{r}''^{\mathrm{T}}\mathbf{e}_1 \\ 0 \end{bmatrix} - \frac{\mathbf{r}'^{\mathrm{T}}\mathbf{e}_1 + \mathbf{r}'^{\mathrm{T}}\mathbf{e}_2}{|\mathbf{r}'|^3}\begin{bmatrix} -\mathbf{r}'^{\mathrm{T}}\mathbf{e}_2 \\ \mathbf{r}'^{\mathrm{T}}\mathbf{e}_1 \\ 0 \end{bmatrix} \tag{37}$$

Eq. (34) can be rewritten as

$$\mathbf{p}' = \mathbf{r}' - yK\mathbf{t}_1 \tag{38}$$

The deformation gradient can thus be conveniently expressed for the beam as

$$\mathbf{F} = \frac{\partial \mathbf{p}}{\partial x} \otimes \mathbf{e}_1 + \frac{\partial \mathbf{p}}{\partial y} \otimes \mathbf{e}_2 + \mathbf{e}_3 \otimes \mathbf{e}_3 = (\mathbf{r}' - yK\mathbf{t}_1) \otimes \mathbf{e}_1 + \mathbf{t}_2 \otimes \mathbf{e}_2 + \mathbf{e}_3 \otimes \mathbf{e}_3 \tag{39}$$

and the Green strain tensor reads

$$\mathbf{E} = \tfrac{1}{2}(\mathbf{F}^{\mathrm{T}}\mathbf{F} - \mathbf{I}) = \tfrac{1}{2}((|\mathbf{r}'| - yK)^2 - 1)\mathbf{e}_1 \otimes \mathbf{e}_1 \tag{40}$$

where $\mathbf{I}$ is the identity matrix. Note that the Green strain tensor only contains one non-vanishing component. It will be used for clarification purposes only in the following: see also Appendix A.

3.3.1. Strain energy based on the polar decomposition and the Biot strain tensor

In order to retrieve the classical elastica equations, the polar decomposition of the deformation gradient is performed. The polar decomposition of a matrix $\mathbf{F}$,

$$\mathbf{F} = \mathbf{R}\mathbf{U} \tag{41}$$

is unique if $\mathbf{R}$ is an orthogonal matrix with $\det(\mathbf{R}) = 1$, representing a rotation matrix, and $\mathbf{U}$ is a positive-semidefinite and symmetric matrix, characterizing the stretch. $\mathbf{U}$ is sometimes called the right Cauchy–Green stretch tensor.

By employing the rotation of the cross section $\mathbf{A}$, see Eq. (32), we find that

$$\begin{aligned}\mathbf{U} = \mathbf{A}^{\mathrm{T}}\mathbf{F} &= (\mathbf{t}_1^{\mathrm{T}}\mathbf{r}' - yK\mathbf{t}_1^{\mathrm{T}}\mathbf{t}_1)\mathbf{e}_1 \otimes \mathbf{e}_1 + \mathbf{e}_2 \otimes \mathbf{e}_2 + \mathbf{e}_3 \otimes \mathbf{e}_3 \\ &= (|\mathbf{r}'| - yK)\mathbf{e}_1 \otimes \mathbf{e}_1 + \mathbf{e}_2 \otimes \mathbf{e}_2 + \mathbf{e}_3 \otimes \mathbf{e}_3 \end{aligned} \tag{42}$$

is already a unique stretch tensor. The diagonal form of the stretch tensor $\mathbf{U}$ fulfills the definitions of the polar decomposition as long as $|\mathbf{r}'| - yK > 0$.

It is convenient to use the stretch tensor $\mathbf{U}$ for the definition of the strain, which leads to the so-called Biot or nominal strain tensor; see e.g. Bažant and Cedolin [24]. The Biot strain tensor is defined as

$$\mathbf{E}^{\mathrm{Biot}} = \mathbf{U} - \mathbf{I} = (\mathbf{F}^{\mathrm{T}}\mathbf{F})^{1/2} - \mathbf{I} \tag{43}$$

Note that $\mathbf{U}$ could be directly computed from Eq. (43) as well. In the Bernoulli–Euler beam, the Biot strain tensor simply reduces to the form

$$\mathbf{E}^{\mathrm{Biot}} = \varepsilon_{11}^{\mathrm{Biot}}\mathbf{e}_1 \otimes \mathbf{e}_1 = (U_{11} - 1)\mathbf{e}_1 \otimes \mathbf{e}_1 = (\varepsilon_0 - yK)\mathbf{e}_1 \otimes \mathbf{e}_1 \tag{44}$$

and provides a much simpler axial strain than the Green strain tensor: see Appendix A.

The Biot strain can be further split into axial resp. bending strain,

$$\varepsilon_0 = |\mathbf{r}'| - 1 \quad \text{and} \quad \varepsilon_{\mathrm{bend}} = yK \tag{45}$$

A recent discussion on the Biot tensor using similar results for the extensible elastica has been given e.g. by Magnusson et al. [25]. It is remarkable that the same axial and bending strain energy can be retained when using the strain definitions of Simo and Vu-Quoc [1] for the case of zero shear deformation.

Eq. (42) can be furthermore interpreted as the linearized Green strain components, defined in a local, corotated cross-section frame. This, often related as a corotational concept, is therefore fully identical to the floating frame of reference formulation, when using a separate floating frame for each point along the beam axis. Géradin and Cardona [5] perform the same projection procedure as provided in Eq. (42) for the shear deformable beam element; however, the rotation of shear strain components only leads to a pseudo-polar decomposition of the deformation gradient.

It is not mentioned by Magnusson et al. [25] that the Biot strain tensor is work conjugate to the Biot stress tensor $\mathbf{T}$ and that the definition of the Biot stress follows from the equivalence of virtual work,

$$\delta w = \mathbf{S} : \delta\mathbf{E} = \mathbf{T} : \delta\mathbf{E}^{\mathrm{Biot}} \tag{46}$$

where $\mathbf{S}$ is the second Piola Kirchhoff stress tensor and $\mathbf{E}$ is the Green strain tensor, which leads to

$$\mathbf{T} = \tfrac{1}{2}(\mathbf{US} + \mathbf{SU}) \tag{47}$$

We assume a linear elastic material of the form,

$$\mathbf{S} = \mathbf{D}^4 : \mathbf{E} \tag{48}$$

with the fourth rank tensor of elasticities $\mathbf{D}^4$. This is also known as the *St. Venant–Kirchhoff material*. The one-dimensional relation simply reads

$$S_{11} = E\varepsilon_{11} \tag{49}$$

where E represents Young's modulus and ε_{11} is the axial component of the Green strain tensor. The one-dimensional form of the Biot stress reads

$$\mathbf{T} = T_{11}\mathbf{e}_1 \otimes \mathbf{e}_1 = U_{11}S_{11}\mathbf{e}_1 \otimes \mathbf{e}_1 \tag{50}$$

which reads, together with the St. Venant–Kirchhoff material of Eq. (48),

$$T_{11} = (\varepsilon_0 + 1 - yK)E\tfrac{1}{2}((\varepsilon_0 + 1 - yK)^2 - 1) \tag{51}$$

The latter equation is highly nonlinear in the transverse coordinate y, the material measure of curvature K and the axial strain ε_0. The St. Venant–Kirchhoff material leads to high coupling of axial deformation and bending

in the virtual work of elastic forces, see Appendix A, independently in which the expression of Eq. (46) is used for virtual work of elastic forces. It is therefore convenient to consider a constitutive modeling in which the Biot stress is a linear function of the Biot strain $\varepsilon_{11}^{\text{Biot}}$. Such a constitutive model in a material model in its own right; compare with Truesdell and Noll [26]. The relation between S_{11} and ε_{11} then turns out to be nonlinear. The constitutive model, linear in T_{11} and $\varepsilon_{11}^{\text{Biot}}$, is well in line with classical nonlinear rod theories and is defined as

$$\bar{T}_{11} = E\varepsilon_{11}^{\text{Biot}} = E(\varepsilon_0 - yK) \tag{52}$$

On the other hand, Eq. (52) might be interpreted as a linearization of the St. Venant–Kirchhoff material assuming $H \ll 1/K$ and $\varepsilon_0 \ll 1$. Finally, we define the virtual work of elastic forces by means of Eq. (52), taking into account the width $W(y)$ of the cross section,

$$\begin{aligned}\delta W_S &= \int_0^L \int_{-H/2}^{H/2} W\bar{T}_{11}\delta\varepsilon_{11}^{\text{Biot}}\,\mathrm{d}y\,\mathrm{d}x \\ &= \int_0^L \int_{-H/2}^{H/2} WE(\varepsilon_0 - yK)\delta(\varepsilon_0 - yK)\,\mathrm{d}y\,\mathrm{d}x \\ &= \int_0^L EA\varepsilon_0\delta\varepsilon_0 - EIK\delta K\,\mathrm{d}x\end{aligned} \tag{53}$$

The resulting virtual work of elastic forces of Eq. (53) is equivalent to the beam formulation of Reissner [2] or Simo and Vu-Quoc [1] when not regarding the shear deformation. The formulation (53) has been proven to obey the principle of frame indifference in the more general shear deformable case [1]. We point out that Eq. (53) is exact in case the material can be prescribed by a linear relation between the Biot stress and the stretch tensor $\mathbf{U}$, which represents an admissible constitutive relation.

The stress resultant in the beam element is defined as the integral of axial stress via the cross section of width W and height H,

$$N = \int_{-H/2}^{H/2} W\bar{T}_{11}\,\mathrm{d}y = \int_{-H/2}^{H/2} WE(\varepsilon_0 - yK)\,\mathrm{d}y = EA\varepsilon_0 \tag{54}$$

where EA is the axial stiffness of the beam element. The normal force is linear in the axial strain ε_0, as opposed to the derivation from the Green strain; see Appendix A. The stress couple is derived in a similar manner by means of

$$M = \int_{-H/2}^{H/2} Wy\bar{T}_{11}\,\mathrm{d}y = \int_{-H/2}^{H/2} WE(y\varepsilon_0 - y^2K)\,\mathrm{d}y = EIK \tag{55}$$

where EI is the bending stiffness. The bending moment is linear in the material measure of curvature K. The same relation can be found in all extensible elastica theories and in the more general nonlinear rod theories [4,2,3,1]; for a more recent work see e.g. Ref. [27].

We are able to treat the case of a pre-stressed or a pre-curved beam element e.g. by subtracting the initial curvature resulting in the bending moment, see also Ref. [2],

$$M = EI(K - K_0) \tag{56}$$

Note that K_0 is equivalent to the initial geometrical curvature of the beam, because the axial coordinate x coincides with the curve-length of the initially curved beam. Eq. (53) might be rewritten equivalently in terms of resultant forces and couples,

$$\delta W_S = \int_0^L N\delta\varepsilon_0 - M\delta K\,\mathrm{d}x \tag{57}$$

3.4. Variation of the axial and bending strain components

For a computer implementation, the variation of the strain components needs to be explicitly formulated with respect to the nodal coordinates. The following equations also demonstrate the simplicity of the absolute nodal coordinate formulation with respect to the equations of motion. The variation of W_S is necessary in the computer implementation, reading

$$\delta W_S = \int_0^L (N\delta\varepsilon_0 + M\delta K)\,\mathrm{d}x \tag{58}$$

The shape function matrix, see Eq. (6), is rewritten in terms of column vectors $\mathbf{S}_i$,

$$\mathbf{S}_m = [\mathbf{S}_1 \dots \mathbf{S}_8] \tag{59}$$

and according to the Einstein summation convention, Eq. (6) can also be rewritten in terms of the nodal coordinates q_i for its spatial derivatives,

$$\mathbf{r} = \mathbf{S}_i q_i, \quad \mathbf{r}' = \mathbf{S}_i' q_i \quad \text{and} \quad \mathbf{r}'' = \mathbf{S}_i'' q_i \tag{60}$$

The variation of the axial strain is given by

$$\delta\varepsilon_0 = \frac{\partial\varepsilon_0}{\partial q_i}\delta q_i = \frac{\mathbf{r}'^{\mathrm{T}}\delta\mathbf{r}'}{|\mathbf{r}'|} = \frac{1}{|\mathbf{r}'|}\mathbf{r}'^{\mathrm{T}}\frac{\partial\mathbf{r}'}{\partial q_i}\delta q_i = \frac{1}{|\mathbf{r}'|}\mathbf{r}'^{\mathrm{T}}\mathbf{S}_i'\delta q_i \tag{61}$$

The variation of K reads

$$\delta K = \frac{\partial}{\partial q_i}\left(\frac{(\mathbf{r}'\times\mathbf{r}'')^{\mathrm{T}}\mathbf{e}_3}{|\mathbf{r}'|^2}\right)\delta q_i = \frac{1}{g^2}\left(g\frac{\partial f}{\partial q_i} - f\frac{\partial g}{\partial q_i}\right)\delta q_i \tag{62}$$

with the placeholders $f = (\mathbf{r}'\times\mathbf{r}'')^{\mathrm{T}}\mathbf{e}_3$ and $g = |\mathbf{r}'|^2$. The derivatives of f and g are given by

$$\frac{\partial f}{\partial q_i} = (\mathbf{S}_i'\times\mathbf{r}'' + \mathbf{r}'\times\mathbf{S}_i'')^{\mathrm{T}}\mathbf{e}_3 \quad \text{and} \quad \frac{\partial g}{\partial q_i} = 2\mathbf{r}'^{\mathrm{T}}\frac{\partial\mathbf{r}'}{\partial q_i} \tag{63}$$

The variation of K finally reads

$$\delta K = \frac{1}{|\mathbf{r}'|^4}[|\mathbf{r}'|^2(\mathbf{S}_i'\times\mathbf{r}'' + \mathbf{r}'\times\mathbf{S}_i'') - 2(\mathbf{r}'\times\mathbf{r}'')(\mathbf{r}'^{\mathrm{T}}\mathbf{S}_i')]^{\mathrm{T}}\mathbf{e}_3\delta q_i \tag{64}$$

3.5. A literature survey on the ANCF using the geometrical curvature

We could find a certainly incomplete number of papers on the absolute nodal coordinate formulation containing a curvature-based strain energy. Most of those works are concerning the Bernoulli–Euler beam theory without shear deformation and an elastic line approach. It is assumed that most of the numerical results presented in those works are correct because the influence of the curvature on the overall deformation is small and because normal forces have not been investigated in detail. However, it is important to mention these works in order to avoid errors made by others in the future. Furthermore, it is important to note that for those ANCF elements which consider a so-called continuum mechanics approach, with the virtual work of elastic forces defined by

$$\delta W_S^{\text{solid}} = \int_V \mathbf{S} : \delta\mathbf{E}\,\mathrm{d}V \tag{65}$$

the following comments do not apply, but the resultant forces should be interpreted according to Appendix A.

3.5.1. The planar case

Concerning the two-dimensional case, Berzeri and Shabana [16] used the curvature for the definition of the strain energy, compare with Eq. (16), which should be replaced. This formulation has been used subsequently

in the papers [16,28,18,10]. It needs to be pointed out that the overall deformation agrees well with physical experiments [28].

An alternative approach is based on a simplified expression for the bending strain based on a corotational evaluation of the linearized curvature [22,29]. As this approach is significantly different from the approach of Ref. [16], it is assumed that the latter papers do not show the above-mentioned problems.

3.5.2. Three-dimensional beam and plate elements

In the three-dimensional case, the coupling of axial deformation, bending, shear and torsion leads to more complicated geometrical relations which have been introduced in an inconvenient manner. In the early days of the developments of the ANCF, Von Dombrowski started with an erroneous expression using the curvatures for the definition of the strain energy, see Ref. [30, Eqs. (35a) and (37b)], while after corotational linearization of the strain components, a reasonable expression follows; see Eq. (42) of [30]. Concerning the derivation given in Ref. [30], the curvatures should be replaced by the expression, e.g. given by Simo [31], reading

$$\boldsymbol{\kappa} = \mathbf{A}^{\mathrm{T}} \frac{\partial \mathbf{A}}{\partial x} \tag{66}$$

where x represents the axial coordinate in reference configuration which is not the arc length of the deformed beam axis. In two works investigating the cross-sectional properties of the absolute nodal coordinate formulation [32,33], the bending strain components should be reconsidered.

In more simple elastic line approaches [34,12,35,36] the curvature should be replaced by K in order to decouple axial strain and bending. In the approach of Schwab and Meijaard, the influence of axial strain has been neglected anyway: see page 6 of Ref. [17]. It is therefore difficult to estimate the size of the error in axial components, but also the latter formulation should be reconsidered with respect to the mentioned problems.

Regarding elastic line approaches for ANCF plate elements, see e.g. Refs. [35,28,37], there are several approximations assuming small inplane deformation. Due to similarities in the formulation of the elastic forces of the thin plate and the thin beams with an elastic line approach, it is suspected that the membrane stresses are erroneous, e.g. in the simple case of the large deformation bending of a cantilever plate.

4. Numerical examples

A large number of examples would be necessary to verify a beam formulation numerically. Following the classical literature on nonlinear beam elements, especially the geometrically exact beam elements, we find several static and dynamic tests, which are frequently used to verify the proposed formulation and which show some significant but also insignificant errors of the conventional formulation of the ANCF beam element. In summary, we subsequently compare the solution of the extensible elastica for the static deformation of a cantilever beam and verify the deformation of a pre-curved beam element with the shape of a half-circle into a exact full circle by means of a torque at the cantilever tip. Hereafter, the classical post-buckling of a 215° arch is studied and, as a dynamical problem, a very flexible pendulum is studied. All computations have been performed in the flexible multibody research code HOTINT [38]. The tolerances have always been set to the utmost possible values, such that the highest accuracy is reached, unless otherwise stated. Time increments of a fixed step-implicit trapezoidal rule are chosen such that the error of the time integration is not reflected in the provided results.

4.1. Investigated beam formulations

In the following examples, up to three different formulations are utilized for the strain energy of the beam element. The first approach is based on the (geometrical) curvature, see Eq. (16), as proposed by '*Berzeri–Shabana*' [16]. The second, and '*proposed approach*' is based on the absolute nodal coordinate formulation with the strain energy derived from the Biot strain tensor, see Eq. (53), which coincides with the extensible elastica and with Reissner's beam formulation when not taking into account shear terms. Note that even if we are using the strain energy according to the geometrically exact formulation [1], there is a significant difference compared to the classical large rotation vector formulation, because no rotations are used in the

present approach. The third approach is derived from a strain energy based on the Green strain and the second Piola Kirchhoff stress with a linear '*St. Venant–Kirchhoff*' material; see Eq. (83) in Appendix A.

4.2. Large deformation of a cantilever beam subjected to a vertical tip load

The static problem of a cantilever beam with a tip load, see Fig. 4, has already been used in the literature for comparison of ANCF beam elements [39] and analytical solutions are available for the Bernoulli–Euler beam. However, none of the provided solutions contains enough digits for a thorough verification and normal forces have not been investigated. It shall be mentioned beforehand that the small deformation results of the cantilever agree well with analytical results of a small deformation beam theory [18].

We derive the iterative solution by means of the extensible elastica theory, as e.g. given by Magnusson et al. [25]. In the elastica theory, the differential equations for a cantilever beam with a vertical tip load are derived from the local equilibrium equations of a stretched beam element,

$$EI\frac{\partial^2\theta(x)}{\partial x^2} = EI\theta'' = -(1+\lambda(x))F_0\cos(\theta(x)) \tag{67}$$

where θ denotes the rotation of the cross section with respect to the undeformed beam coordinate and λ denotes the axial elongation, given for the cantilever beam as

$$\lambda(x) = \frac{F_0}{EA}\sin(\theta(x)) \tag{68}$$

The horizontal distance between the tip and the support, denoted by l_f, see Fig. 4, results from the (unknown) rotation and stretch of the beam segment, given by the integral

$$l_f = \int_0^L [(\lambda+1)\cos(\theta(x)) + 1]\,\mathrm{d}x \tag{69}$$

The bending moment at the support is thus given by

$$M_0 = F_0 l_f \tag{70}$$

The values of θ and θ' therefore take on the following values at the support:

$$\theta(0) = 0 \quad \text{and} \quad \theta'(0) = M_0/EI \tag{71}$$

We now implement the differential equation (67) in MAPLE 9.5 [20] and iteratively solve the angle $\theta^{(i)}(s)$ at iteration i with the given bending moment $M_0^{(i-1)}$ of the last iteration. Due to the ability of MAPLE to calculate with arbitrary digits, we are able to produce reference solutions with arbitrary accuracy. We use 22 digits for the calculation which is sufficient to obtain 16 converged digits of accuracy. In fact, the comparison of a large number of digits is necessary, because when using the wrong expressions for the curvature, it is possible to obtain accurate displacements up to several digits, depending on the problem, but there always

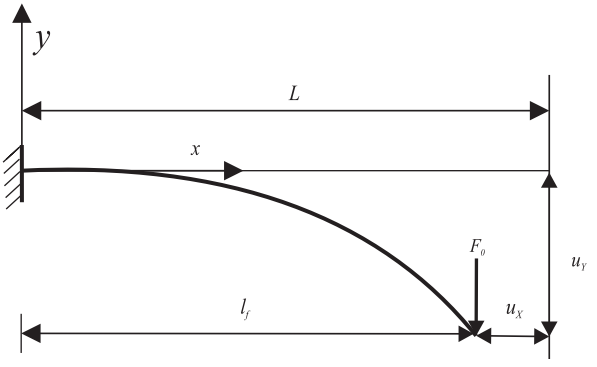

Fig. 4. Cantilever beam subjected to end load.

Table 1
Axial and transverse displacement of the tip of the cantilever beam using the proposed ANCF approach, see Eq. (53), and comparison to the analytical solution of the extensible elastica

Elements	u_x	u_y
1	0.362244729891	0.994144758725
2	0.488926308341	1.175222865055
4	0.507428715119	1.205533702233
8	0.508509236497	1.207197756020
16	0.508536579844	1.207238894935
32	0.508537277691	1.207239826397
64	0.508537302970	1.207239853336
128	0.508537304246	1.207239854483
256	0.508537304321	1.207239854546
512	0.508537304326	1.207239854550
1024	0.508537304326	1.207239854550
Ext. elastica	0.5085373043258772	1.207239854549824

Table 2
Converged axial and transverse tip-displacements of the cantilever beam under tip load using the proposed, the Berzeri–Shabana and the St. Venant–Kirchhoff approach with 512 elements

formulation	u_x	u_y
Proposed approach	0.508537304326	1.207239854550
Berzeri–Shabana	0.5089228704	1.2083981311
St. Venant–Kirchhoff	0.5085521768	1.2073298486
Ext. elastica	0.508537304326	1.207239854550

remains a small error, see e.g. the investigation presented by Dibold et al. [18]. This forced us to look at converged solutions which are presented in the following.

The numerical data for the cantilever consists of length $L = 2\,\mathrm{m}$, rectangular cross section $h = b = 0.1\,\mathrm{m}$ and Young's Modulus $E = 2.07\mathrm{e}+11\,\mathrm{N/m^2}$. The tip load has been chosen according to $F_0 = 3EI/L^2$, which leads to very large displacements. Table 1 shows the results for the proposed case using the modified strain energy given in Eq. (53). It turns out that the proposed element coincides with the classical extensible Euler elastica solution for at least 12 digits using 1024 elements (depending on the numerical solver and the machine accuracy which is typically $1\mathrm{e}-16$). Table 2 shows converged results for the proposed approach, see Eq. (53), the Berzeri–Shabana approach, see Eq. (16), the approach with the St. Venant–Kirchhoff material, see Eq. (83), and a comparison with the classical extensible elastica solution. It turns out that the Berzeri–Shabana approach leads to results which match neither the elastica solution nor the consistent approach based on the St. Venant–Kirchhoff material. The error of the Berzeri–Shabana element is approximately 10^{-3} even in the converged case. While this error in the tip displacement is insignificant in many technical problems, it might be important when verifying results or comparing two different theories. It is necessary to point out that the smaller difference between the elastica solution and the St. Venant–Kirchhoff solution is based on the differences in the material law, and it turns out that the difference becomes smaller for smaller height of the beam (for $h = 0.1\,\mathrm{m}$, the difference is about 3×10^{-5} and for $h = 0.01\,\mathrm{m}$, the difference is only 3×10^{-7}).

The speed of convergence in the proposed element is shown in the logarithmic error plot of Fig. 5. The rate of convergence has at least order four, which is one order higher than the interpolation order of the shape functions: see Eq. (7). The element therefore shows excellent performance in highly nonlinear problems.

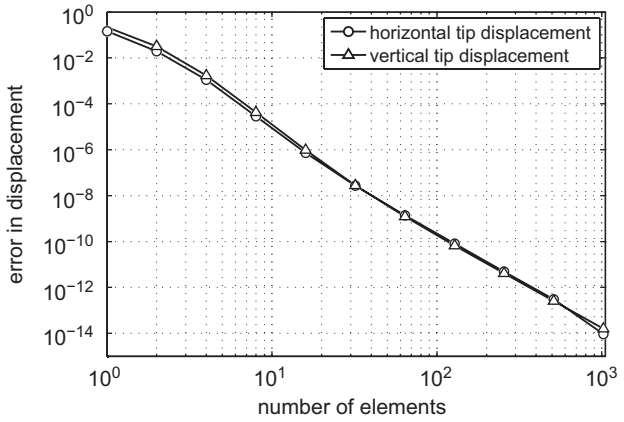

Fig. 5. Convergence of the horizontal and vertical tip displacement of the cantilever with the proposed formulation.

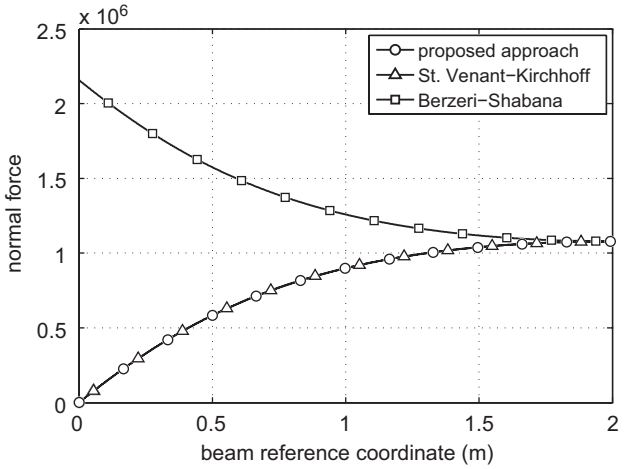

Fig. 6. Normal force in the cantilever beam for different formulations of the bending strain energy.

A much more serious error of the original formulation has been found in the normal force of the beam element. Fig. 6 shows the normal force in the cantilever beam for different formulations, using the respective expression for each formulation to evaluate the normal force. The proposed approach is based on the extensible elastica and classical nonlinear rod theory: see Eq. (53) with the normal force according to Eq. (54). The second formulation is based on the St.Venant–Kirchhoff material without any geometrical approximations, using Green strain and second Piola–Kirchhoff stress, see Eq. (83), with the normal force from Eq. (79). The third formulation is according to Berzeri and Shabana: see Eq. (16) together with Eq. (20). The standard static example of a cantilever shows that small approximations in the axial deformations can lead to significant errors in the stress resultants or the strain. The error in the normal force using the original beam formulation of Berzeri and Shabana is found to be approximately

$$N_{\text{err}} \approx EI\kappa^2 \tag{72}$$

and it is independent of the mesh size; cf. Eq. (30). It is also of utmost importance to note that for the case of the St.Venant–Kirchhoff material, a simplified normal force $F = EA\varepsilon_{11}^0$, instead of Eq. (79), leads to similar errors in the normal force.

Fig. 7 shows the appropriate bending moment in the cantilever beam for different formulations of the strain energy. Apparently, the investigated formulations agree very well for the bending moment. This is the reason why terms of the size $|\mathbf{r}'|$ are neglected frequently.

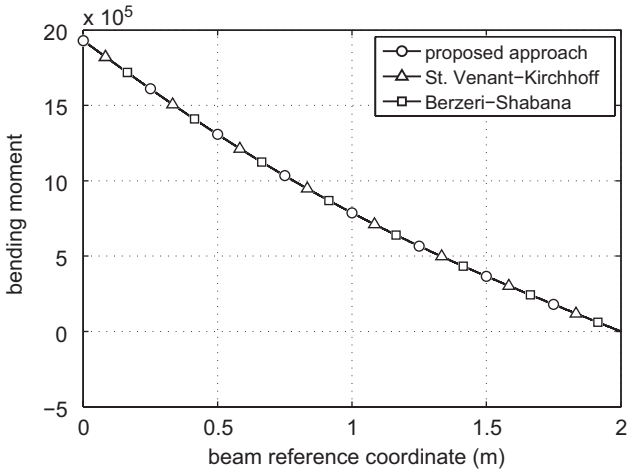

Fig. 7. Bending moment in the cantilever beam for different formulations of the bending strain energy.

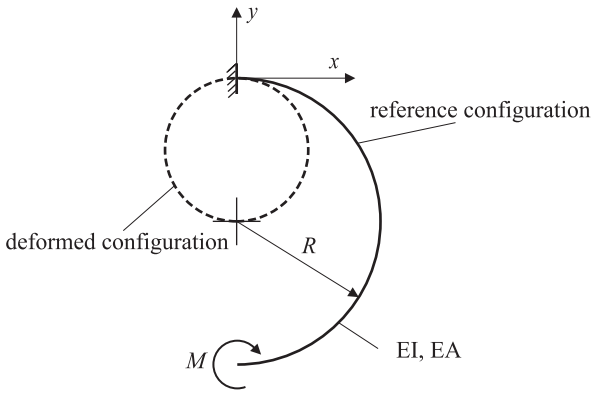

Fig. 8. Half-circle cantilevered beam subjected to bending moment at the free end.

4.3. Bending of a pre-curved beam into a full circle

In the second example, the static deformation of a pre-curved beam element is investigated: see Fig. 8. A cantilever beam with the initial shape of a half-circle is bent into a full circle by means of a torque applied at the free end. According to the Bernoulli–Euler beam theory, a torque of

$$M = EI\frac{\pi}{L} = EIR \tag{73}$$

is applied to bend the curved beam into a full circle. We investigate the convergence of the position of the free end, which should finally have the position $(x = 0, y = 0)$. A similar example has been studied by Ibrahimbegovic [40]. Compared to the latter reference, we use other geometrical and material parameters in order to demonstrate the difference of the proposed formulations for the bending strain. However, because the example is scalable and the exact solution is known, the results are quite comparable.

The parameters of the beam are bending stiffness $EI = 10^5\,\mathrm{N/m^2}$, axial stiffness $EA = 5 \times 10^8\,\mathrm{N}$ and radius $R = 1\,\mathrm{m}$.

The nonlinear solver, based on the full Newton method, needs two loading increments and a total of 14 Newton iterations to obtain the converged solution (relative residual tolerance $\mathrm{tol} = 10^{-6}$) for the problem discretized with 40 elements and using the proposed bending strain energy of Eq. (57). The geometrically exact beam element according to Simo and Vu-Quoc is also reported to require two loading increments in order to

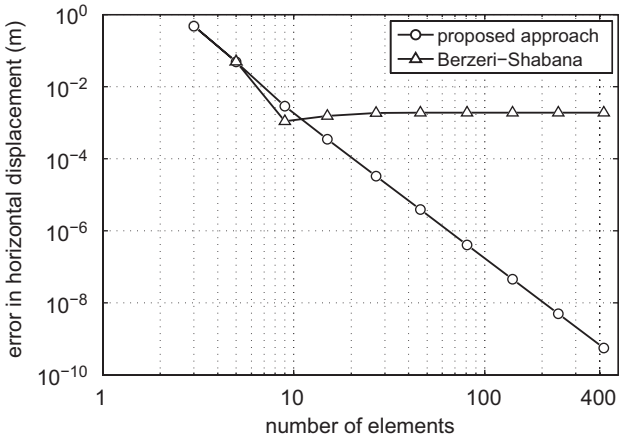

Fig. 9. Error in the horizontal (x) displacement of the tip of the circular beam versus number of elements.

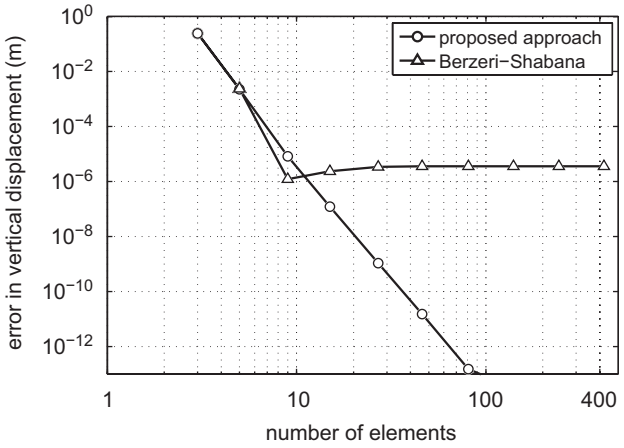

Fig. 10. Error in the vertical (y) displacement of the tip of the circular beam versus number of elements.

obtain the full circle: see Ibrahimbegovic [40]. In the case of the Berzeri–Shabana approach, see Eq. (16), a total number of at least five loading increments are needed in order to obtain the solution of the bent circle, using 37 Newton iterations. The higher number of loading increments could result from the inconsistency in the bending strain.

Figs. 9 and 10 show the error of the horizontal and vertical displacement of the tip of the half-circle cantilever beam subjected to a bending moment at the tip. The analytical solution should give exactly zero. The errors are normalized to the original radius R of the half-circle. The results show that the incorrect usage of the curvature in the bending strain energy causes an error in the deformation of a beam even in the converged case and even if the axial extension should not be present or should not play an important role in this example. The error of the vertical deformation is much smaller than the error of the horizontal deformation, because the error in the bending/extension of the beam leads to large horizontal, but only small vertical displacements. It should be mentioned that the number of elements n to discretize the circle has been chosen according to $n = 3^{(i/2)}$ for $i = 2 \ldots 11$ and truncating non-integer numbers. This avoids the possibility that a discretization with (2^i) elements could eventually lead to a much faster convergence than just any odd or even number (accounting for the symmetry of the problem).

Fig. 11 furthermore shows the axial strain in the beam element for the proposed approach and the Berzeri–Shabana approach: see Eq. (16). The solution is calculated using 1024 elements for the discretization of the half-circle where the axial strain is converged. It is apparent that the beam element using the curvature

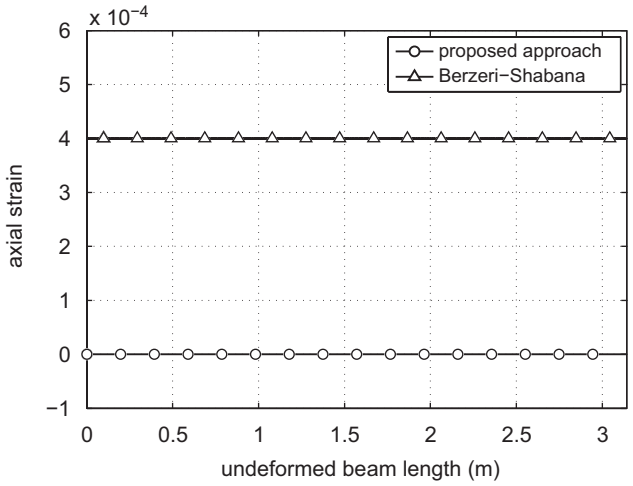

Fig. 11. Axial strain in the circular beam versus the undeformed beam length.

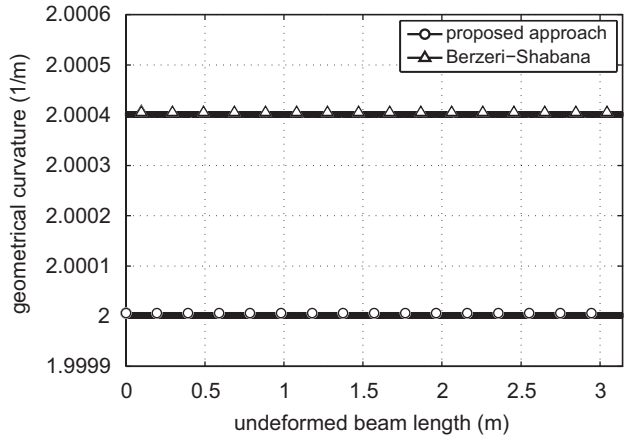

Fig. 12. Curvature in the circular beam versus the undeformed beam length.

shows erroneous axial extension, which follows exactly the analytical value derived in Eq. (30). The same plot for the geometrical curvature shows a slight difference from the exact solution, see Fig. 12, resulting from the difference in axial deformation; cf. Eq. (30). In both cases, the curvature is not fully constant, but oscillates slightly for every element. This is a natural effect in finite elements, caused by the low-order approximation of the bending strain. It shall be noted that several authors already attempted to solve the even simpler problem of bending a straight beam into a circle; see e.g. Refs. [39,33]. However, they did not show the converged results by means of numerical values and neither did they show convergence plots for the error.

4.4. *Post-buckling of a* 215° *arch*

In the following section we compare the present beam formulation with a well-known example from the literature. The post-buckling of arches with different angles has been studied extensively by DaDeppo and Schmidt [41] using the inextensible elastica beam theory. The results for the critical loads have been used by researchers in order to validate numerical models for nonlinear beam formulations: see Simo and Vu-Quoc [8] or Ibrahimbegovic [40]. The latter author provides additional parameters for the axial stiffness to approximate the inextensibility condition, which are used in the present study. According to Fig. 13, the parameters of the

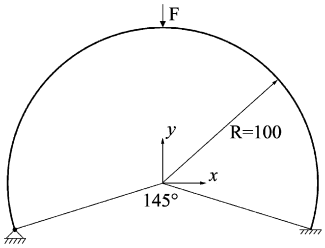

Fig. 13. 215° arch with unsymmetric boundary conditions under vertical loading.

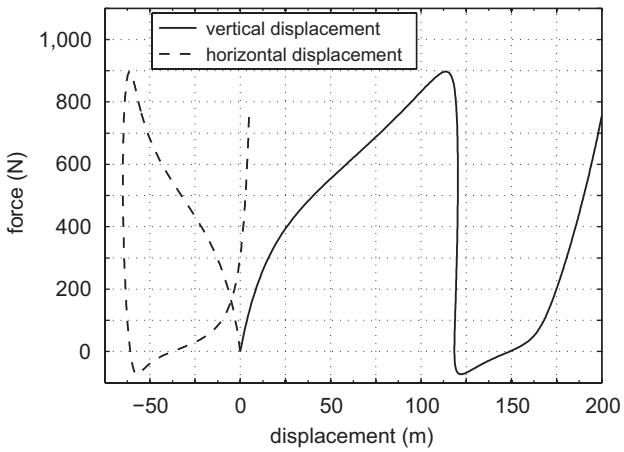

Fig. 14. Load versus displacement trace of the nonlinear equilibrium path in the circular arch.

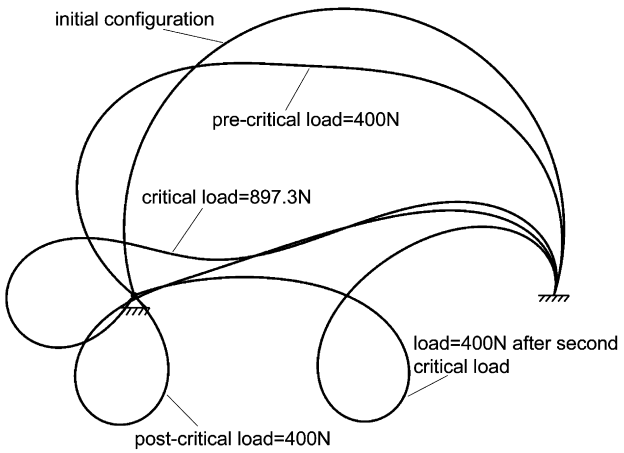

Fig. 15. Intitial, deformed and post-buckling configuration (snap-through) of a 215° arch.

arch are bending stiffness $EI = 10^6\,\mathrm{N/m^2}$, axial stiffness $EA = 10^8\,\mathrm{N}$ and radius $R = 100\,\mathrm{m}$. The circular arch spans 215° of a circle and is fixed at the right support and hinged at the left support.

The nonlinear static computation is performed such that the loading is increased as long as an equilibrium can be reached, the value found hereafter gives a good approximation of the buckling load. Fig. 14 shows the displacements of the equilibrium path of the point of load F for the pre- and post-buckling case. The load–displacement curves could be tracked by a variable load/displacement control for the nonlinear static solver. Fig. 15 shows several different states during the pre- and post-buckling phase of the arch problem.

Table 3
Critical buckling load versus the number of elements in the large deformation 215° arch problem

Elements	Critical load (N)	
	Proposed approach	Berzeri–Shabana
32	904.570	904.548
64	898.012	897.989
128	897.314	897.290
256	897.295	897.272
DaDeppo and Schmidt [41]	897	
Simo and Vu-Quoc [8]	905.28	
Ibrahimbegovic [40]	897.3	

Table 4
Comparison of eigenfrequencies (Hz) for the proposed ANCF beam element versus analytical solution

Mode	Number of elements				Analytical
	10	20	40	80	
1	26.51	25.09	24.90	24.89	24.891
2	80.61	71.57	70.44	70.40	70.401
3	168.25	138.66	135.12	134.98	134.988
4	249.06	226.77	218.64	218.30	218.305
5	541.17	336.68	320.96	320.26	320.249
6	774.92	469.62	442.14	440.80	440.782

Note that there are three different configurations shown for a load of $F = 400\,\mathrm{N}$; cf. Fig. 14. Fig. 15 agrees well with the results of Simo and Vu-Quoc [8] and Géradin and Cardona [5].

Table 3 shows the critical loading values for the first buckling versus the number of elements with the proposed approach, see Eq. (57), and the Berzeri–Shabana approach; see Eq. (16). There are only slight differences between these two methods, because axial deformation is very small. The results are also compared to values provided in the literature [41,8,40] which are equal up to the provided number of digits, except for the result of Simo and Vu-Quoc [8], where only linear elements have been used and therefore their results are not converged. We also studied the case of a reduced axial stiffness of $EA = 10^5\,\mathrm{N}$, where the difference of the investigated methods is much higher, leading to a value of $F_{\mathrm{crit}} = 883.9\,\mathrm{N}$ for the proposed and $F_{\mathrm{crit}} = 862.8\,\mathrm{N}$ for the Berzeri–Shabana approach; see Eq. (16).

4.5. Dynamic example: eigenfrequencies of a circular beam

Regarding the linear analysis of a pre-curved beam element that has been designed for large deformation analysis, it is a good test to investigate the eigenfrequencies of a full circle modeled with Bernoulli–Euler beam elements. The numerical parameters are copied from a previous study related to the absolute nodal coordinate formulation [33], using the radius $r = 0.5\,\mathrm{m}$, axial stiffness $EA = 2 \times 10^8\,\mathrm{N}$, bending stiffness $EI = \frac{1}{6} \times 10^4\,\mathrm{N\,m^2}$ and mass density $\rho A = 7.85\,\mathrm{kg/m}$. The analytical solution, see Ref. [33], does not consider axial deformation. However, due to the very high axial stiffness, a good agreement is expected. Due to the same reason, only the proposed approach is investigated, while the alternative approaches give almost the same results. Table 4 shows the normalized first 6 eigen-frequencies versus the number of elements used to discretize the circle. The frequencies of rigid body modes are not included in Table 4 but are included in the beam model. In comparison with the results presented by Sugiyama and Suda [33], we obtain much better agreement with the analytical values by using quite few elements.

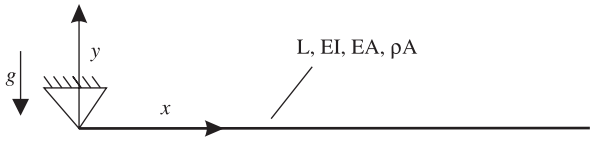

Fig. 16. Initial configuration of the very flexible pendulum.

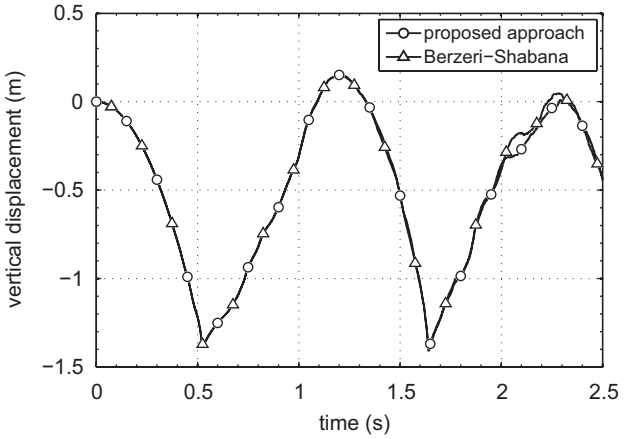

Fig. 17. Vertical displacement versus time of a very flexible pendulum, comparing the proposed and the Berzeri–Shabana approach.

Table 5
Vertical displacement (m) in the very flexible pendulum using the proposed approach (PA) and the approach by Berzeri and Shabana (BS)

Time (s)	128 elem. (BS)	128 elem. (PA)	256 elem. (PA)
0.528	−1.37414	−1.37389	−1.37389
1.210	0.15393	0.15065	0.15068
2.100	−0.17696	−0.26818	−0.26806
2.250	0.02181	−0.03613	−0.03683

4.6. Dynamic example, energy conservation: large deformation pendulum

In the last example, the free falling of a very flexible pendulum under the effect of gravity according to Berzeri and Shabana [16] is considered. The data of the pendulum, see Fig. 16, consist of length $L = 1.2\,\mathrm{m}$, area $A = 0.0018\,\mathrm{m}^2$, area moment of inertia $I = 1.215 \times 10^{-8}\,\mathrm{m}^4$, Young's modulus $E = 0.7 \times 10^6\,\mathrm{N}$, density $\rho = 5540\,\mathrm{kg/m}^3$ and gravity $g = 9.81\,\mathrm{m/s}^2$.

Fig. 17 shows the vertical displacement versus time, which visually agrees well with the reference paper [16]. A quite large number of 128 elements have been utilized for the discretization of the beam, about ten times more than in the reference computation [16]. A comparison with 256 elements showed that both solutions are already converged, indicating no visible difference. Nevertheless, the proposed approach based on the geometrically exact beam theory leads to slightly different results compared to the previous approach based on curvature. Table 5 provides certain values for the vertical displacement for certain times as a reference for subsequent investigations, and the difference of the investigated approaches is apparent.

Fig. 18 finally shows the kinetic, potential and total energy during the free falling of the pendulum. Potential energy consists of strain energy and change of potential energy within the field of gravity. In a study over a longer time period, the conservation properties are still found to be satisfied. As compared to geometrically exact approaches with rotational degrees of freedom, the present approach based on absolute nodal

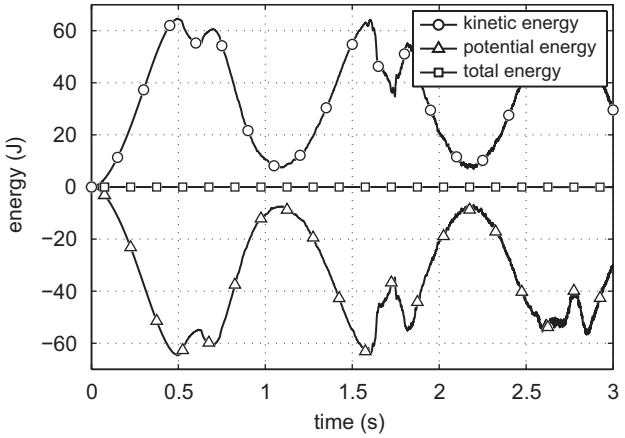

Fig. 18. Conservation of energy in the very flexible pendulum using the proposed approach.

(displacement) coordinates does not require energy-momentum-conserving algorithms to obtain stable integration.

5. Conclusion

A detailed analysis and comparison of the proposed ANCF beam finite element and classical nonlinear rod theories has been presented. As a consequence of good agreements of these theories, also in the numerical examples, it is appropriate to claim that the absolute nodal coordinate formulation can give the same results as the elastica theories as well as the geometrically exact beam element of Simo and Vu-Quoc [1], when disregarding shear deformation. It has been shown that the proposed consistent strain terms are different from the formulation of Berzeri and Shabana [16], and that the latter formulation leads to wrong stress resultants and buckling loads and requires more nonlinear iterations. The proposed formulation does not contain rotations, the finite element has a constant mass matrix even in the extension to the three-dimensional case and achieves at least a convergence order of three for the displacements. Additionally, we examined the original absolute nodal coordinate formulation which is based on the Green Lagrange strain and the second Piola Kirchhoff stress with a St. Venant–Kirchhoff material. We were able to show the differences of the latter formulation and the classical nonlinear rod theories on a beam kinematical level without approximations other than the Bernoulli–Euler conditions. The formulation is currently extended to the shear deformable case which is planned to be published in the near future.

Acknowledgments

Support of the authors by the K2-Austrian Center of Competence in Mechatronics, ACCM, and of J. Gerstmayr by the Academy of Finland, Grant No. [108397], is gratefully acknowledged.

Appendix A. Bernoulli–Euler beam theory for the St. Venant–Kirchhoff material

The following derivation is intended to show the differences of the virtual work derived in Section 3.3.1 and a derivation based on a linear relation between the Green strain and the second Piola–Kirchhoff stress, subsequently denoted as the St. Venant–Kirchhoff approach. An alternative discussion on the Green strain in the beam theory has been performed by Géradin and Cardona [5, p. 112ff].

The Green strain tensor reads for the Bernoulli–Euler beam element with the kinematical description of Eq. (31),

$$\mathbf{E} = \tfrac{1}{2}((|\mathbf{r}'| - yK)^2 - 1)\mathbf{e}_1 \otimes \mathbf{e}_1 \tag{74}$$

see also Eq. (40). The only non-zero axial component of the Green strain can thus be written as

$$\varepsilon_{11} = \tfrac{1}{2}(|\mathbf{r}'|^2 - 1 - 2y|\mathbf{r}'|K + y^2K^2) = \varepsilon_{11}^0 - y|\mathbf{r}'|K + \tfrac{1}{2}y^2K^2 \tag{75}$$

which shows constant, linear and quadratic terms with respect to the transverse coordinate y: see also Fig. 2. Note that the abbreviation $\varepsilon_{11}^0 = \frac{1}{2}(|\mathbf{r}'|^2 - 1)$ is used.

Considering a linear elastic material in the form of the St. Venant–Kirchhoff law, see Eq. (48), the second Piola–Kirchhoff stress becomes for the one-dimensional case,

$$S_{11} = E(\varepsilon_{11}^0 - y|\mathbf{r}'|K + \tfrac{1}{2}y^2K^2) \tag{76}$$

A frequent method to define the "normal force" is to integrate the second Piola–Kirchhoff stress via the cross section, which leads to the interesting result

$$N^{(P2)} = \int_{-H/2}^{H/2} WE\left(\varepsilon_{11}^0 - y|\mathbf{r}'|K + \frac{1}{2}y^2K^2\right)\mathrm{d}y = EA\varepsilon_{11}^0 + \frac{1}{2}EIK^2 \tag{77}$$

However, the latter result does not provide a resultant force, e.g. for applying boundary conditions. Following the classical rod theories [3], appropriate stress resultants and stress couples are derived from the first Piola–Kirchhoff stress tensor [42], which is denoted as $\mathbf{P}$,

$$\mathbf{P} = \mathbf{FS} = (\varepsilon_{11}^0 - y|\mathbf{r}'|K + \tfrac{1}{2}y^2K^2)(|\mathbf{r}'| - yK)\mathbf{t}_1 \otimes \mathbf{e}_1 \tag{78}$$

The normal force can be derived from the local differential equilibrium equations integrated along the cross section. The stress resultant in the St. Venant–Kirchhoff formulation must thus be written as

$$\begin{aligned} N^{(P1)} &= \int_{-H/2}^{H/2} WES_{11}F_{11}\mathbf{t}_1\,\mathrm{d}y \\ &= \int_{-H/2}^{H/2} WE\left(\varepsilon_{11}^0 - y|\mathbf{r}'|K + \frac{1}{2}y^2K^2\right)(|\mathbf{r}'| - yK)\,\mathrm{d}y \\ &= EA\varepsilon_{11}^0|\mathbf{r}'| + \tfrac{3}{2}EIK^2|\mathbf{r}'| \end{aligned} \tag{79}$$

The latter result shows that, in contrast to classical results, the normal force involves strong coupling of strain at the beam centerline, ε_{11}^0, and bending deformation, K. It furthermore leads to the conclusion that there is no permanent neutral (undeformed) fiber in a beam that is subjected to pure bending. The normal force of Eqs. (77) and (79) does not coincide with the cross-sectional area times axial stress at the beam axis. It is possible to define an averaged axial Green strain in the Bernoulli–Euler beam by integrating Eq. (75) over the cross section,

$$\varepsilon_0^{(G)} = \frac{1}{A}\int_{-H/2}^{H/2} W\left(\varepsilon_{11}^0 - y|\mathbf{r}'|K + \frac{1}{2}y^2K^2\right)\mathrm{d}y = \varepsilon_{11}^0 + \frac{1}{2}\frac{EI}{EA}K^2 \tag{80}$$

Using Eq. (79) in order to evaluate the normal force in the numerical example in Section 4.2 leads to good agreement with the results of classical nonlinear rod theories, see Fig. 6, while Eq. (77) may unfortunately lead to erroneous results, i.e. negative strain in a tensioned beam.

Similar relations follow for the stress couple, where the first Piola–Kirchhoff stress is again utilized to define the bending moment which follows after some calculations,

$$M^{(P1)} = \int_{-H/2}^{H/2} WyES_{11}F_{11}\,\mathrm{d}y = -EIK|\mathbf{r}'|^2 + \frac{1}{2}EI_4K^3 \tag{81}$$

Note that only quadratic and fourth-order terms in y survive the integration over the cross section. The fourth-order term in y leads to a fourth-order moment of inertia denoted as EI_4, which demonstrates that the St. Venant–Kirchhoff material leads to non-classical expressions. For a rectangular cross section, the additional term reads $EI_4 = EWH^5/80$. A possible bending strain-related term derived from the Green strain

tensor is defined as

$$K^{(G)} = -\frac{1}{I}\int_{-H/2}^{H/2} W\left(\varepsilon_{11}^0 - y|\mathbf{r}'|K + \frac{1}{2}y^2K^2\right) y\,\mathrm{d}y = K|\mathbf{r}'| \tag{82}$$

It is again interesting that the bending-related strain is coupled in axial deformation $|\mathbf{r}'|$ and the material measure of curvature K. The virtual work of elastic forces for a St. Venant–Kirchhoff (SVK) material can be derived in analogy to Eq. (53) by means of

$$\begin{aligned}\delta W_S^{\mathrm{SVK}} &= \int_0^L \int_{-H/2}^{H/2} WS_{11}\delta\varepsilon_{11}\,\mathrm{d}y\,\mathrm{d}x \\ &= \int_0^L \int_{-H/2}^{H/2} WE\left(\varepsilon_{11}^0 - y|\mathbf{r}'|K + \frac{1}{2}y^2K^2\right)\delta\left(\varepsilon_{11}^0 - y|\mathbf{r}'|K + \frac{1}{2}y^2K^2\right)\mathrm{d}y\,\mathrm{d}x \\ &= \int_0^L \left[EA\varepsilon_{11}^0\delta\varepsilon_{11}^0 + EI\left((3\varepsilon_{11}^0+1)K\delta K + \frac{3}{2}K^2\delta\varepsilon_{11}^0\right) + EI_4\frac{1}{2}K^3\delta K\right]\mathrm{d}x\end{aligned} \tag{83}$$

Eq. (83) shows a high coupling of ε_{11}^0 and K, which is undesired from a computational point of view and makes a term-by-term interpretation difficult. Eq. (83) reflects the beam kinematical relations of the classical absolute nodal coordinate formulation for the planar and shear-rigid case.

Equivalently, it is possible to use the deformation gradient $\mathbf{F}$ to define appropriate axial resp. bending "strains" which are work-conjugate to the first Piola–Kirchhoff stress resultants; see Eqs. (79) and (81). The virtual strains are denoted as $\delta\varepsilon_0^{(F)}$ resp. $\delta K^{(F)}$ and are defined as

$$\begin{aligned}\delta\varepsilon_0^{(F)} &= \frac{1}{A}\int_{-H/2}^{H/2} W\delta(|\mathbf{r}'| - yK)\,\mathrm{d}y = \delta|\mathbf{r}'|, \\ \delta K^{(F)} &= -\frac{1}{I}\int_{-H/2}^{H/2} Wy\delta(|\mathbf{r}'| - yK)\,\mathrm{d}y = \delta K\end{aligned} \tag{84}$$

The similarity to the strains of the geometrically exact beam formulation, see Eq. (45), is remarkable, however, the difference from the latter formulation is based on different stress resultants.

Finally, it shall be noted that the virtual work of elastic forces can be represented by means of the virtual work of first Piola–Kirchhoff stress resultants and the virtual strain resultants based on the deformation gradient,

$$\delta W_S^{\mathrm{SVK}} = \int_0^L N^{(P1)}\delta\varepsilon_0^{(F)} + M^{(P1)}\delta K^{(F)}\,\mathrm{d}x \tag{85}$$

which is equivalent to Eq. (83).

Remarks to the St. Venant–Kirchhoff approach:

- Eq. (83) does not take into account any approximations and can be thus understood as a geometrically exact formulation. However, the correct introduction of virtual work for external torques and forces seems to be cumbersome. The formulation does not have the simplicity which is sometimes preferred for the analysis of engineering structures.
- The fully parametrized beam element based on the absolute nodal coordinate formulation [7] is based on the same strain energy as Eq. (83), while additionally including shear deformation and torsion. The newly derived relations of normal force and bending moment, see Eqs. (79) and (81), should also be considered in the fully parameterized element.
- Due to the occurrence of the fourth-order moment of inertia EI_4, it is obvious that Eq. (83) is elementarily different from the formulation based on the elastica, given by Eq. (57). It can thus be concluded that the fully parameterized ANCF beam element [7] is based on a conceptually different beam formulation from classical nonlinear rod theories [3,2]. For example, Eq. (83) does not lead to a permanent neutral fiber in pure bending.

- When considering material nonlinearities, it is convenient to extend Eq. (76) similar as done in classical solid finite element formulations and the respective strain energy and resultant forces can be derived.
- For the case of small axial deformation, Eqs. (83) and (57) lead to very similar results for the deformation and the resultant forces, see e.g. the numerical examples.

References

[1] J.C. Simo, L. Vu-Quoc, On the dynamics of flexible beams under large overall motions—the plane case: parts I and II, *Journal of Applied Mechanics* 53 (1986) 849–863.

[2] E. Reissner, On one-dimensional finite strain beam theory: the plane problem, *Journal of Applied Mathematics and Physics* 23 (1972) 794–804.

[3] S.S. Antman, *The Theory of Rods, Handbuch der Physik*, Vol. VIa/2, Springer, Berlin, 1972.

[4] A.E.H. Love, *A Treatise on the Mathematical Theory of Elasticity*, Dover, New York, 1944.

[5] M. Géradin, A. Cardona, *Flexible Multibody Dynamics—A Finite Element Approach*, Wiley, New York, 2001.

[6] A.A. Shabana, Definition of the slopes and the finite element absolute nodal coordinate formulation, *Multibody System Dynamics* 1 (1997) 339–348.

[7] R.Y. Yakoub, A.A. Shabana, Three dimensional absolute nodal coordinate formulation for beam elements, *ASME Journal of Mechanical Design* 123 (2001) 606–621.

[8] J.C. Simo, L. Vu-Quoc, A three-dimensional finite-strain rod model, part II: computational aspects, *Computer Methods in Applied Mechanis and Engineering* 58 (1986) 79–116.

[9] L.G. Maqueda, A.A. Shabana, Nonlinear constitutive models and the finite element absolute nodal coordinate formulation, *Proceedings of the IDETC/CIE 2007*, Las Vegas, ASME, New York, 2007; Paper No. DETC2007-34521.

[10] M. Stangl, J. Gerstmayr, H. Irschik, A large deformation finite element for pipes conveying fluid based on the absolute nodal coordinate formulation, *Proceedings of the IDETC/CIE 2007*, Las Vegas, ASME, New York, 2007; Paper No. DETC2007-34771.

[11] J.T. Sopanen, A.M. Mikkola, Description of elastic forces in absolute nodal coordinate formulation, *Nonlinear Dynamics* 34 (2003) 53–74.

[12] J. Gerstmayr, A.A. Shabana, Analysis of thin beams and cables using the absolute nodal coordinate formulation, *Nonlinear Dynamics* 45 (1–2) (2006) 109–130.

[13] J. Gerstmayr, M.K. Matikainen, Improvement of the accuracy of stress and strain in the absolute nodal coordinate formulation, *Mechanics Based Design of Structures and Machines* 34 (4) (2006) 409–430.

[14] J. Gerstmayr, J. Schöberl, A 3D finite element method for flexible multibody systems, *Multibody System Dynamics* 15 (2006) 309–324.

[15] J. Gerstmayr, J.A.C. Ambrósio, Component mode synthesis with constant mass and stiffness matrices applied to flexible multibody systems, *International Journal for Numerical Methods in Engineering*, available online doi:10.1002/nme.2133.

[16] M. Berzeri, A.A. Shabana, Development of simple models for the elastic forces in the absolute nodal co-ordinate formulation, *Journal of Sound and Vibration* 235 (4) (2000) 539–565.

[17] A.L. Schwab, J.P. Meijaard, Comparison of three-dimensional flexible beam elements for dynamic analysis: finite element method and absolute nodal coordinate formulation, *Proceedings of the IDETC/CIE 2005*, Long Beach, ASME, New York, 2005; Paper No. DETC2005-85104.

[18] M. Dibold, J. Gerstmayr, H. Irschik, On the accuracy and computational costs of the absolute nodal coordinate and the floating frame of reference formulation in deformable multibody systems, *Proceedings of the IDETC/CIE 2007*, Las Vegas, ASME, New York, 2007; Paper No. DETC2007-34756.

[19] H. Irschik, J. Gerstmayr, A continuum mechanics based derivation of Reissner's large-displacement finite–strain beam relations: the case of plane, originally straight Bernoulli–Euler beams, *Acta Mechanica*, submitted for publication.

[20] MAPLE 9.5, Maplesoft, Waterloo Maple Inc., 615 Kumpf Drive, Waterloo, ON, Canada, April 7, 2004. www.maplesoft.com.

[21] M.A. Omar, A.A. Shabana, A two-dimensional shear deformable beam for large rotation and deformation problems, *Journal of Sound and Vibration* 243 (3) (2001) 565–576.

[22] J.L. Escalona, H.A. Hussien, A.A. Shabana, Application of the absolute nodal coordinate formulation for flexible multibody system dynamics, *Journal of Sound and Vibration* 214 (5) (1998) 833–851.

[23] S.S. Antman, *Nonlinear Problems of Elasticity*, Springer, New York, 1995.

[24] Z.P. Bažant, L. Cedolin, *Stability of Structures*, Oxford University Press, Oxford, 1991.

[25] A. Magnusson, M. Ristinmaa, C. Ljung, Behavior of the extensible elastica solution, *International Journal of Solids and Structures* 38 (2001) 8441–8457.

[26] C. Truesdell, W. Noll, *The Non-Linear Field Theories of Mechanics*, third ed., Springer, New York, 2004.

[27] G. Jelenić, M.A. Crisfield, Geometrically exact 3D beam theory: implementation of a strain-invariant finite element for statics and dynamics, *Computer Methods in Applied Mechanics and Engineering* 171 (1999) 141–171.

[28] W.-S. Yoo, S.-J. Park, O.N. Dmitrochenko, D.Yu. Pogorelov, Verification of absolute nodal coordinate formulation in flexible multibody dynamics via physical experiments of large deformation problems, *Journal of Computational and Nonlinear Dynamics* 1 (2006) 81–93.

[29] R. Iwai, N. Kobayashi, A new flexible multibody beam element based on the absolute nodal coordinate formulation using the global shape function and the analytical mode shape function, *Nonlinear Dynamics* 34 (2003) 207–232.

[30] S. Von Dombrowski, Analysis of large flexible body deformation in multibody systems using absolute coordinates, *Multibody System Dynamics* 8 (2002) 409–432.
[31] J.C. Simo, A finite strain beam formulation, the three-dimensional dynamic problem, part I, *Computer Methods in Applied Mechanics and Engineering* 49 (1985) 55–70.
[32] H. Sugiyama, J. Gerstmayr, A.A. Shabana, Deformation modes of the finite element cross section, *Journal of Sound and Vibration* 298 (2006) 1129–1149.
[33] H. Sugiyama, Y. Suda, A curved beam element in the analysis of flexible multi-body systems using the absolute nodal coordinates, *Proceedings of the Institution of Mechanical Engineers Part K: Journal of Multi-body Dynamics* 221 (2007) 219–231.
[34] J. Gerstmayr, A.A. Shabana, Analysis of higher and lower order elements for the absolute nodal coordinate formulation, *Proceedings of the IDETC/CIE 2005*, Long Beach, ASME, New York, 2005; Paper no. DETC2005-84827.
[35] O.N. Dmitrochenko, D.Yu. Pogorelov, Generalization of plate finite elements for absolute nodal co-ordinate formulation, *Multibody System Dynamics* 10 (2003) 17–43.
[36] O.N. Dmitrochenko. A new finite element of a thin spatial beam in absolute nodal coordinate formulation, in: J.M. Goicolea, J. Cuadrado, J.C. García Orden (Eds.), *Multibody Dynamics 2005—ECCOMAS Thematic Conference*, Madrid, 2005 (CDROM).
[37] K. Dufva, A.A. Shabana, Analysis of thin plate structures using the absolute nodal coordinate formulation, *Proceedings of the Institution of Mechanical Engineers Part K: Journal of Multi-body Dynamics* 219 (2005) 345–355.
[38] http://tmech.mechatronik.uni-linz.ac.at/staff/gerstmayr/hotint.html
[39] K. Dufva, J.T. Sopanen, A.M. Mikkola, A two-dimensional shear deformable beam element based on the absolute nodal coordinate formulation, *Journal of Sound and Vibration* 280 (2005) 719–738.
[40] A. Ibrahimbegović, On finite element implementation of geometrically nonlinear Reissner's beam theory: three-dimensional curved beam elements, *Computer Methods in Applied Mechanics and Engineering* 122 (1995) 11–26.
[41] D.A. DaDeppo, R. Schmidt, Instability of clamped-hinged circular arches subjected to a point load, *Transactions of the ASME* 97 (3) (1975) 894–896.
[42] D.F. Parker, On the derivation of nonlinear rod theories from three-dimensional elasticity, *Journal of Applied Mathematics and Physics* 35 (1984) 833–847.